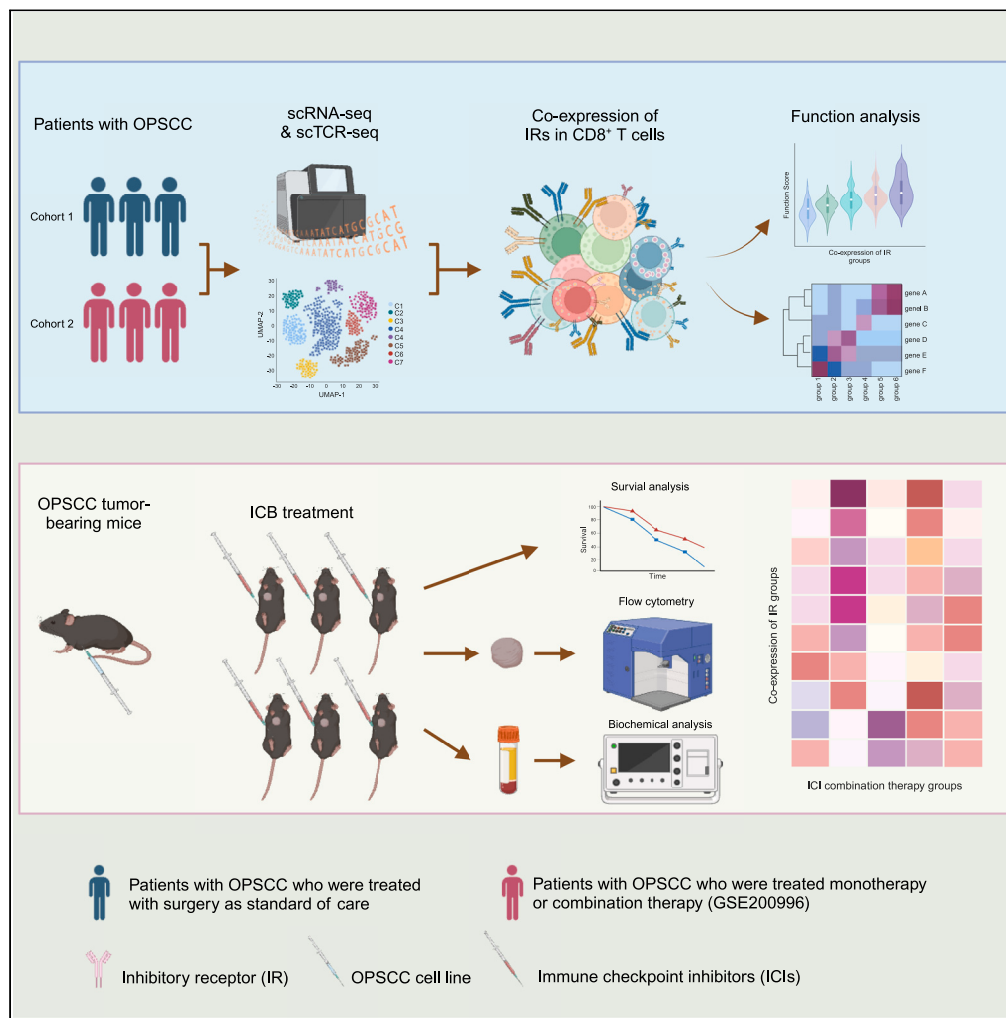


Article

# The diversity of inhibitory receptor co-expression patterns of exhausted CD8<sup>+</sup> T cells in oropharyngeal carcinoma



Yufang Rao, Ke Qiu, Yao Song, ..., Haopeng Yu, Yu Zhao, Jianjun Ren

yutzhao@vip.163.com (Y.Z.)  
jianjun.ren@scu.edu.cn (J.R.)

**Highlights**

Highly diverse IR co-expression is a leading feature of exhausted CD8<sup>+</sup> T cells

A higher number of co-expressed IRs indicates superior anti-tumor potential

Individual and dual ICB redistribute the IR co-expression patterns



## Article

The diversity of inhibitory receptor co-expression patterns of exhausted CD8<sup>+</sup> T cells in oropharyngeal carcinoma

Yufang Rao,<sup>1,10</sup> Ke Qiu,<sup>1,10</sup> Yao Song,<sup>1,10</sup> Minzi Mao,<sup>1,10</sup> Lan Feng,<sup>1</sup> Danni Cheng,<sup>1</sup> Junhong Li,<sup>1</sup> Ziyang Zhang,<sup>1</sup> Yuyang Zhang,<sup>1</sup> Xiuli Shao,<sup>1</sup> Wendu Pang,<sup>1</sup> Yan Wang,<sup>2</sup> Xuemei Chen,<sup>2</sup> Chuanhuan Jiang,<sup>2</sup> Sisi Wu,<sup>2</sup> Shuaishuai Yu,<sup>2</sup> Jun Liu,<sup>1</sup> Haiyang Wang,<sup>1</sup> Xingchen Peng,<sup>3</sup> Lin Yang,<sup>4</sup> Li Chen,<sup>4</sup> Xiaosong Mu,<sup>5</sup> Yongbo Zheng,<sup>1</sup> Wei Xu,<sup>6</sup> Geoffrey Liu,<sup>7,8</sup> Fei Chen,<sup>1</sup> Haopeng Yu,<sup>9</sup> Yu Zhao,<sup>1,\*</sup> and Jianjun Ren<sup>1,11,\*</sup>

## SUMMARY

**Exhausted CD8<sup>+</sup> T cells (Texs) are characterized by the expression of various inhibitory receptors (IRs), whereas the functional attributes of these co-expressed IRs remain limited. Here, we systematically characterized the diversity of IR co-expression patterns in Texs from both human oropharyngeal squamous cell carcinoma (OPSCC) tissues and syngeneic OPSCC model. Nearly 60% of the Texs population co-expressed two or more IRs, and the number of co-expressed IRs was positively associated with superior exhaustion and cytotoxicity phenotypes. In OPSCC patients, programmed cell death-1 (PD-1) blockade significantly enhanced *PDCD1*-based co-expression with other IR genes, whereas dual blockades of PD-1 and cytotoxic T lymphocyte-associated protein 4 (CTLA-4) significantly upregulated *CTLA4*-based co-expression with other IR genes. Collectively, our findings demonstrate that highly diverse IR co-expression is a leading feature of Texs and represents their functional states, which might provide essential clues for the rational selection of immune checkpoint inhibitors in treating OPSCC.**

## INTRODUCTION

The global incidence of oropharyngeal squamous cell carcinoma (OPSCC) has substantially increased, particularly in cases of human papillomavirus (HPV) infections.<sup>1–3</sup> Despite recent progress in immunotherapy,<sup>4</sup> our understanding of the highly heterogeneous T cell exhaustion states in tumor microenvironments (TME) and diverse responses of OPSCC to immunotherapy remains limited.<sup>5</sup>

Inhibitory receptors (IRs), including programmed cell death-1 (PD-1), lymphocyte activation gene 3 (LAG3), and anti-cytotoxic T lymphocyte-associated antigen 4 (CTLA-4), play crucial roles in regulating T cell responses and have emerged as promising targets in cancer immunotherapy.<sup>6,7</sup> The spectrum of T cell exhaustion ranges from highly proliferative T cells to the complete loss of effector function and replicative capacity, typically characterized by elevated and sustained expression of IRs.<sup>8–11</sup>

Accumulating evidence indicates that the diversity of IR co-expression among T cells may be essential in addressing resistance to single or dual immunotherapy.<sup>12</sup> No consensus exists regarding the functional attributes of IR co-expression with varying expression levels, amounts, and combinations. Some researchers consider IR co-expression as an indication of T cell exhaustion, whereas others claim it defines a subset of activated and functional effector cells.<sup>12–14</sup> For example, early exhausted PD-1<sup>+</sup> T cells (Tex) cells can be reinvigorated by anti-programmed cell death-ligand 1 (PD-L1) treatment, whereas terminally exhausted Tex cells expressing PD-1, LAG3, or TIM3 are unresponsive to anti-PD-1 or PD-L1 treatment.<sup>15</sup> The impact on anti-tumor response and potential change of co-expression pattern of IRs after immune checkpoint inhibitor (ICI) treatment remains unclear.

<sup>1</sup>Department of Otolaryngology-Head & Neck Surgery, West China Hospital, Sichuan University, Chengdu, Sichuan, China

<sup>2</sup>Research Core Facility of West China Hospital, Sichuan University, Chengdu, China

<sup>3</sup>Department of Biotherapy and National Clinical Research Center for Geriatrics, Cancer Center, West China Hospital, Sichuan University, Chengdu, Sichuan, China

<sup>4</sup>MinSheng Ear-Nose-Throat Hospital, Chengdu, Sichuan, China

<sup>5</sup>Langzhong People's Hospital, Nanchong, Sichuan, China

<sup>6</sup>Department of Biostatistics, Princess Margaret Cancer Centre and Dalla Lana School of Public Health, Toronto, ON, Canada

<sup>7</sup>Medical Oncology and Hematology, Princess Margaret Cancer Centre, and Department of Medicine, University of Toronto, Toronto, ON, Canada

<sup>8</sup>Department of Medicine, Division of Medical Oncology and Hematology, Princess Margaret Cancer Center, University Health Network, University of Toronto, Toronto, ON, Canada

<sup>9</sup>West China Biomedical Big Data Center, West China Hospital, Sichuan University, Chengdu, China

<sup>10</sup>These authors contributed equally

<sup>11</sup>Lead contact

\*Correspondence: yutzhao@vip.163.com (Y.Z.), jianjun.ren@scu.edu.cn (J.R.)

<https://doi.org/10.1016/j.isci.2024.109668>



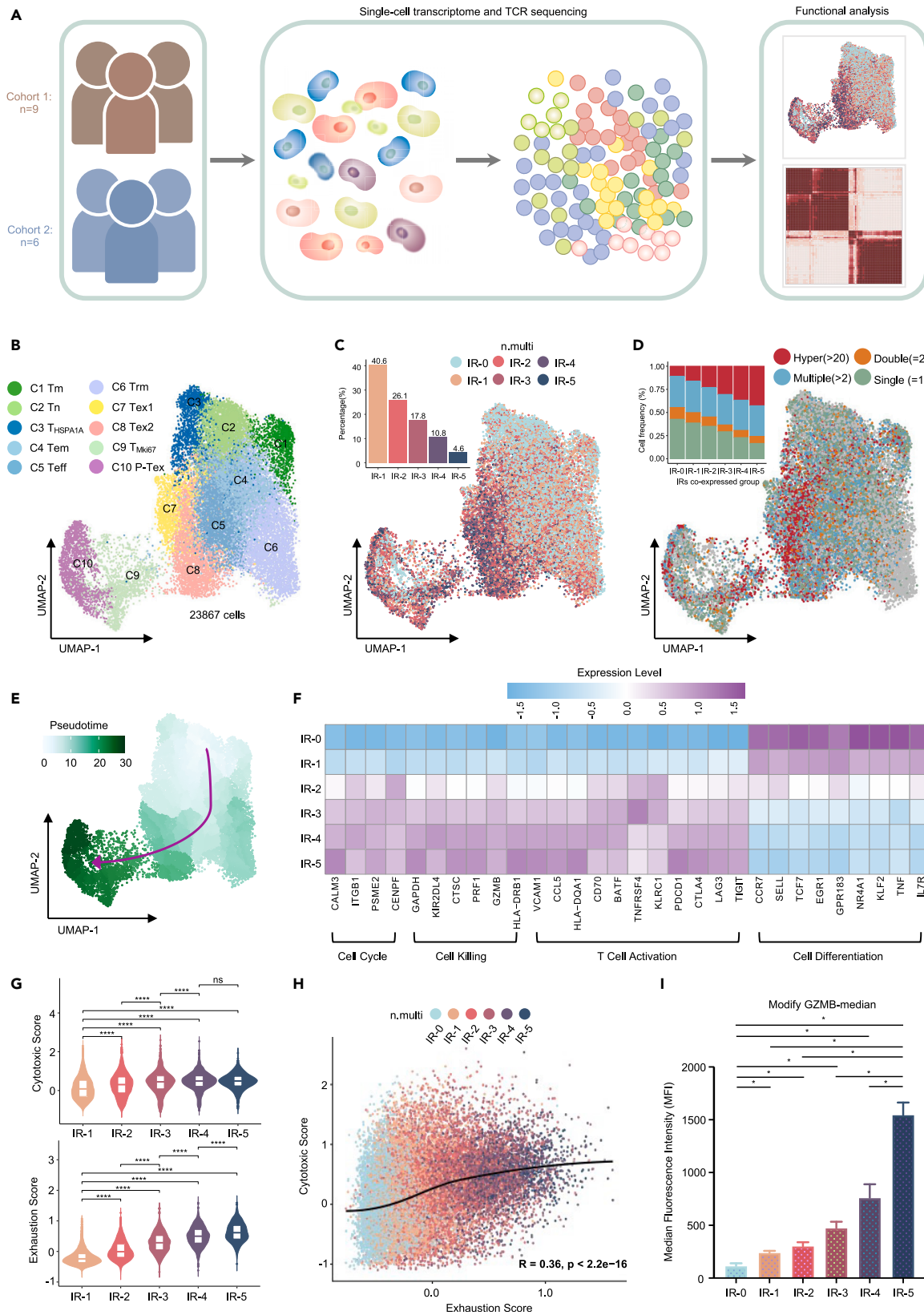


**Figure 1. Co-expression of multiple IRs is positively associated with superior exhausted and cytotoxic phenotype**

- (A) The experimental workflow of sample acquisition, processing, and analyses for single-cell RNA and TCR clonality. Cohort 1 of patients with OPSCC who were treated with surgery as standard of care, and dataset of cohort 2 generated from GSE200996, of which patients with OPSCC underwent monotherapy with  $\alpha$ -PD-1 mAb (nivolumab) or combination therapy with two doses of PD-1 mAb and a single infusion of  $\alpha$ -CTLA-4 mAb (ipilimumab). The numbers of each cohort are denoted.
- (B) UMAP plot showing the sub-clusters of CD8<sup>+</sup> T cells, including interleukin 7 receptor-positive (*IL7R*<sup>+</sup>) memory cells (C1, Tm cells), selectin L-positive (*SELL*<sup>+</sup>) naive cells (C2, Tn cells), heat shock protein family A member 1A-positive (*HSPA1A*<sup>+</sup>) T cells (C3, *T<sub>HSPA1A</sub>*), granzyme K-positive (*GZMK*<sup>+</sup>) effector memory cells (C4, Tem cells), perforin 1-positive (*PRF1*<sup>+</sup>) effector cells (C5, Teff cells), *ZNF683*<sup>+</sup> tissue-resident memory cells (C6, Trm cells), two *PDCD1*<sup>+</sup> (gene for PD-1) exhausted cell populations (C7–C8, Tex cells), and two *MKI67*<sup>+</sup> (gene for Ki67) proliferative exhausted cell populations (C9–C10, P- Tex cells).
- (C) UMAP plot showing the distribution of co-expression inhibitory receptors (IRs) in CD8<sup>+</sup> T cells. Bar graph (top left) showing the proportion of each IRs co-expression group among all CD8<sup>+</sup> T cells. IR-0 indicates cell cluster in which none of the five inhibitory receptors were detected, IR-1 denotes cell cluster in which only one of the five inhibitory receptors was expressed, and so on. IR-2 to IR-5 represents the different cell clusters in which any two to five inhibitory receptor combinations were expressed.
- (D) UMAP plot showing the distribution of single-cell TCR clonotype frequency. Hyper indicates TCR clonotypes shared by more than 20 cells. Bar graph showing the proportion of TCR clonotypes in each IRs co-expressed group.
- (E) Developmental trajectory of CD8<sup>+</sup> T cell subsets inferred by Monocle3.
- (F) Heatmap showing the expression levels of selected gene signatures in each IRs co-expression group.
- (G) Violin plots showing the function scores of cytotoxicity (top) and exhaustion (bottom) of each IRs co-expression group. *p* values obtained by Wilcoxon multiple comparison tests. \**p* < 0.05, \*\**p* < 0.01, \*\*\**p* < 0.001, and \*\*\*\**p* < 0.0001.
- (H) Scatterplot showing the Spearman correlation between cytotoxic score and exhaustion score in IRs<sup>+</sup> cells.
- (I) Flow cytometry analysis showing the median fluorescence intensity (MFI) of GZMB on IRs<sup>+</sup> cells in untreated tumor-bearing mice. Statistics were assessed by Tukey's multiple comparison tests.

Our study aimed to systematically investigate the co-expression diversity of various IRs in the Tex cells of patients with OPSCC. First, we examined the co-expression levels, amounts, and combinations of IRs, analyzing their functional attributes. We compared these patterns among different tissue origins, HPV status, and tumor stages in human OPSCC tissue samples. Subsequently, alterations in the co-expression patterns of several IRs were analyzed, following single and dual co-blockades in patients with OPSCC.

**RESULTS****Co-expression of multiple IRs is positively associated with superior exhausted and cytotoxic phenotype**

To decipher the complexity of the TME in OPSCC, single-cell RNA sequencing (scRNA-seq) profiles were generated for eight primary tumors and five adjacent normal tissues from nine patients with treatment-naïve OPSCC, using 10× Genomics platform (Figure 1A; Table S1). After quality control, 23,867 CD8<sup>+</sup> T cells were extracted based on initial clustering and cell type identification. Unsupervised clustering analysis was performed on the CD8<sup>+</sup> T cells using the Seurat software, and 10 clusters were annotated (C1–10) with canonical marker genes (Figures 1B and S1A; Table S2).<sup>16–19</sup> The distribution of cell clusters for each patient matched well with that of the other patients, suggesting minimal batch effect variability due to sample processing (see STAR Methods).

Notably, the expression levels of typical immune checkpoint molecules, including *PDCD1*, *CTLA-4*, *LAG3*, *TIGIT*, and *HAVCR2*, and several suppressive molecules (including *ENTPD1*, *LAYN*, *TOX*, *CXCL13*, *TNFRSF9*, *LAIR1*, and *KLRC1*) were determined in these CD8<sup>+</sup> T cell subclusters, revealing predominant expression in exhausted cell populations (C7–C10), except for *LAIR1* and *KLRC1*, which were not expressed (Figure S1B; Table S3). We systematically characterized the distribution of IRs co-expressed in CD8<sup>+</sup> T cells. Two or more co-expressed IRs accounted for nearly 60% (approximately 59.4%) of the exhausted cell populations, whereas only 40.6% were single-positive IR (C7–C10, Figure 1C). Clonality analysis based on T cell receptor sequencing data indicated a positive association between the proportion of hyper-expanded CD8<sup>+</sup> T cells and the number of co-expressed IRs (Figure 1D). Pseudotime trajectory analysis consistently revealed that the differentiation trajectory correlated with an increased number of co-expressed IRs, indicating that the co-expression levels of IRs partially reflected the activation and maturation status of CD8<sup>+</sup> T cells (Figure 1E).<sup>20</sup> To further clarify the potential influence of co-expressed IRs on the function of CD8<sup>+</sup> T cells, we systematically characterized the expression patterns of functional genes based on their co-expression levels. The results showed that cells co-expressing IR-0 and IR-1 showed high functionality in *cell differentiation*, whereas those co-expressing more than two IRs showed significant functions in *T cell activation*, *cell killing*, and *cell cycle* (Figure 1F). Cytotoxicity and exhaustion scores were calculated to quantitatively assess the functional differences between CD8<sup>+</sup> T cells with different IR co-expression levels. Higher cytotoxicity and exhaustion scores were associated with an increased number of co-expressed IRs (Figure 1G; Table S4).<sup>21,22</sup> Additionally, we observed that the cytotoxicity and exhaustion scores were positively correlated ( $R^2 = 0.36$ ,  $p < 0.05$ ; Figure 1H). To further verify the observed associations between the co-expression levels of IRs and cytotoxicity at the proteomic level, surface staining of the five inhibitory receptors (*PDCD1*, *CTLA-4*, *LAG3*, *TIGIT*, *HAVCR2*) and intracellular staining of GZMB (a representative effector molecule for cytotoxicity) were performed on tumor-infiltrated CD8<sup>+</sup> T cells from untreated OPSCC tumor-bearing mice. As expected, GZMB expression positively correlated with the number of co-expressed IRs (Figure 1I).

These results suggest a positive association between the amount of co-expressed IRs and the exhausted and cytotoxic phenotypes of CD8<sup>+</sup> T cells.

**Distribution patterns of co-expressed IRs in CD8<sup>+</sup> T cells**

To systematically illustrate the influence of certain clinical characteristics on the co-expression levels of IRs in CD8<sup>+</sup> T cells, a subgroup analysis was conducted based on tissue origin, HPV status, and tumor stage. Subgroup analysis showed that CD8<sup>+</sup> T cells co-expressing two or more

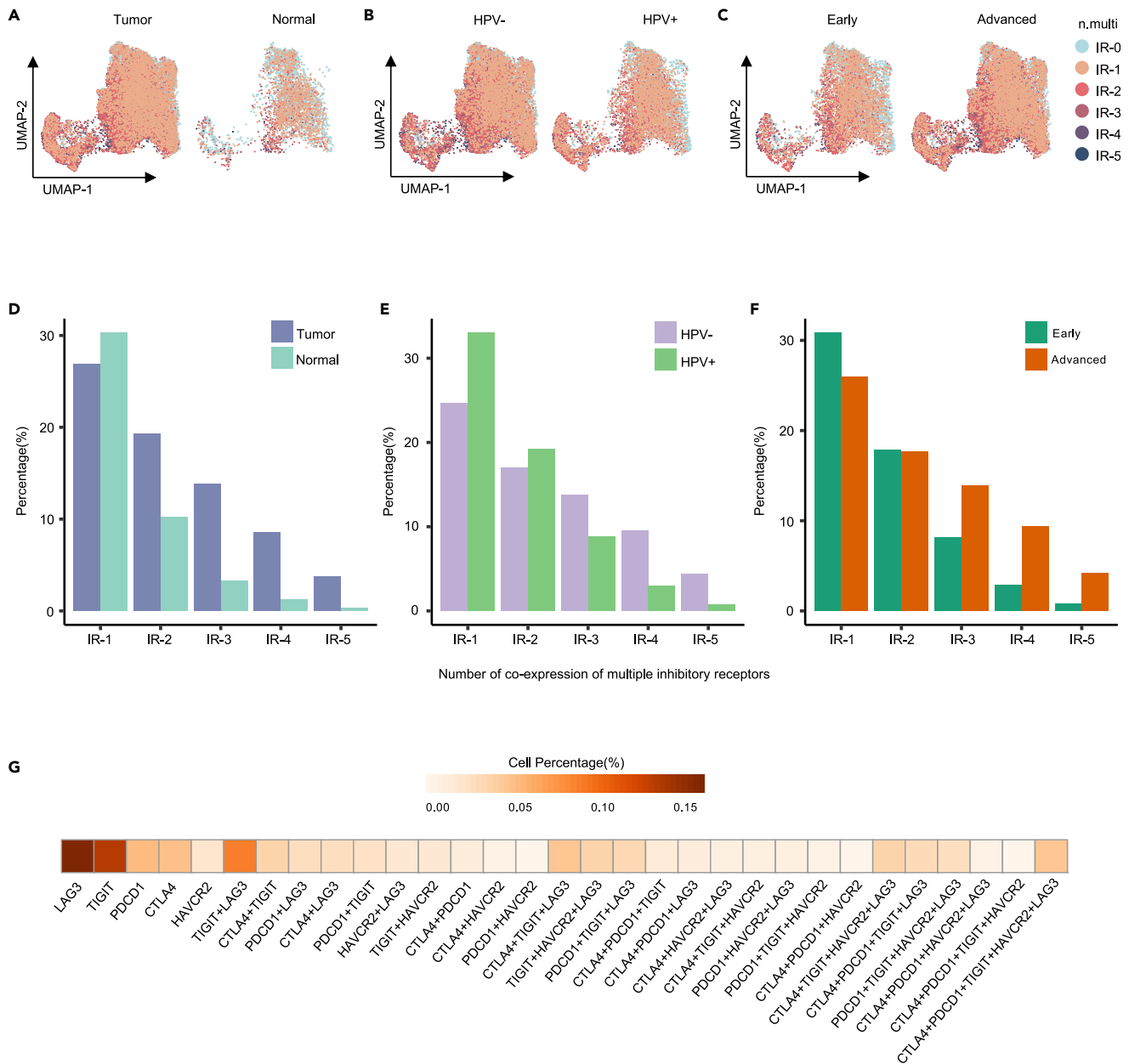


**Figure 2. Distribution patterns of co-expressed IRs in CD8<sup>+</sup> T cells**

(A–C) UMAP plots showing the distribution of IR<sup>+</sup> cells in different tissue origin.

(D–F) Bar graphs showing the proportion of each IRs co-expression group among tissue origin (D), tissue HPV status (E), and tissue T stage (F).

(G) Heatmap showing the proportion of each possible individual IR expression profile.

IRs were more frequently found in tumors (versus adjacent normal tissues), HPV-negative samples (vs. HPV-positive samples), and tumors with advanced stage (vs. tumors with early stage) (Figures 2A–2F and S2A; Table S5). Further investigation into the abundance of specific combinations of co-expressed IRs in CD8<sup>+</sup> T cells showed that LAG3 had the highest single-positive IR. For double-, triple-, and quadruple-positive co-expression of IRs, the most common combinations of CD8<sup>+</sup> T cells in patients with OPSCC were LAG3<sup>+</sup>TIGIT<sup>+</sup>, LAG3<sup>+</sup>TIGIT<sup>+</sup>CTLA-4<sup>+</sup>, and CTLA4<sup>+</sup>TIGIT<sup>+</sup>HAVCR2<sup>+</sup>LAG3<sup>+</sup> (Figure 2G).

Conclusively, the distribution patterns of co-expressed IRs in CD8<sup>+</sup> T cells varied according to tissue origin, HPV status, and tumor stage, whereas LAG3-based IR combinations were the most prevalent in CD8<sup>+</sup> T cells, indicating that targeting these IR combinations may improve the response to immunotherapy.

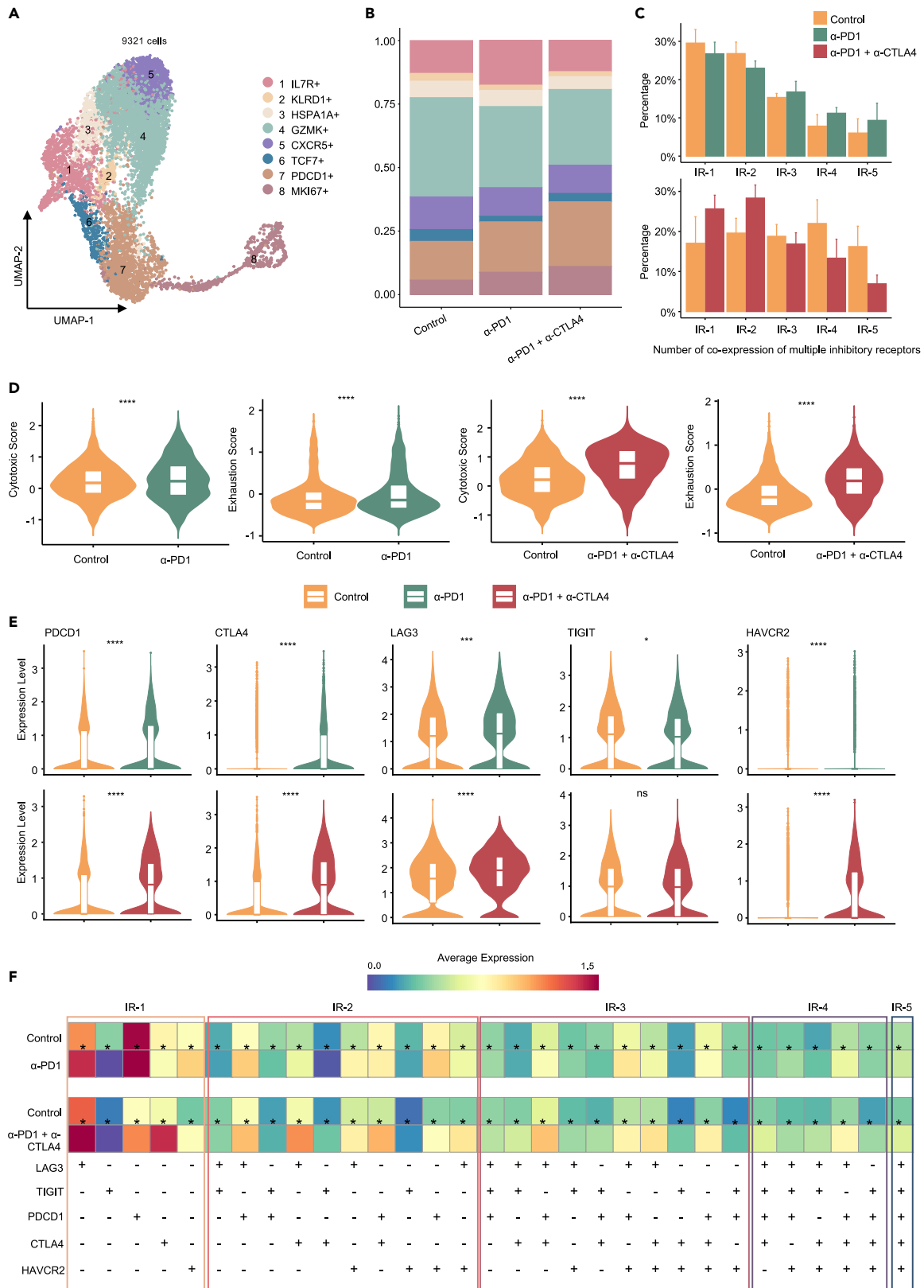


**Figure 3. Individual- and dual blockades of PD-1 and CTLA-4 redistributed the IR co-expression patterns in CD8<sup>+</sup> T cells**

- (A) UMAP plots showing the distribution of infiltrated CD8<sup>+</sup> T cell clusters across pre- and post-treatment groups.
- (B) Bar graph showing the fraction of each cluster in control, individual ( $\alpha$ -PD-1), and dual ( $\alpha$ -PD1 and  $\alpha$ -CTLA4) IR blockade groups.
- (C) Bar graphs showing the percentage of IR cells in control, individual, and dual blockade groups.
- (D) Violin plots showing the altered expression level of specific IRs after receiving individual or dual ICB (paired Wilcox test, \*\*\* $p \leq 0.001$ , \*\*\*\* $p \leq 0.0001$ ).
- (E) Violin plots showing the function score between control, individual, and dual IR blockade groups.
- (F) Heatmap showing the altered average expression level of each IR co-expression patterns after receiving individual or dual ICB (all comparisons are significant).

**Individual and dual blockades of PD-1 and CTLA-4 redistributed the IR co-expression patterns in CD8<sup>+</sup> T cells**

Previous studies have established that ICIs, including anti-PD-1 and anti-CTLA-4, can block the exhaustion process and reinvigorate the function of CD8<sup>+</sup> T cells.<sup>12,23,24</sup> However, the alteration in expression patterns of IRs after ICIs treatment remains unclear. Therefore, we extracted and re-analyzed the published scRNA-seq data of tumor-infiltrating CD8<sup>+</sup> T cells collected from patients with OPSCC who underwent ICIs treatment before surgery ( $n = 6$  patients: three received monotherapy with PD-1 mAb and three with combination therapy involving PD-1 mAb and CTLA-4 mAb; all patients underwent pre-treatment biopsies<sup>25</sup>).

Eight subclusters were identified in these tumor-infiltrating CD8<sup>+</sup> T cells (9,321 cells, Figure 3A; Table S6), and the subclusters were annotated as previously described (see STAR Methods). The proportion of Tex and P-Tex clusters was higher in tumors receiving anti-PD-1 treatment and combination therapy comprising anti-PD-1 and anti-CTLA-4 (Figure 3B). A comparison of matched pre- and post-treatment specimens demonstrated that the percentages of CD8<sup>+</sup> T cells co-expressing three or more IRs (IR-3, IR-4, and IR-5) increased in the anti-PD-1 treatment group. In contrast, the cell fraction of CD8<sup>+</sup> T cells co-expressing one or two IRs (IR-1 and IR-2) increased in the combination therapy group (Figure 3C), consistent with CTLA-4 acting at the priming phase of the immune response to enhance T cell activation. At the same time, PD-1 regulates the function of previously activated cells.<sup>26</sup>

Next, we quantitatively assessed whether ICI treatment altered CD8<sup>+</sup> T cell function. The results showed that both individual and dual blockades of PD-1 and CTLA-4 significantly increased the cytotoxicity and exhaustion scores (Figure 3D; Tables S7 and S8). All functional genes were identical to those shown in Figure 1G. We further characterized the changes in the expression levels of each IR. Similarly, all IRs were expressed at higher levels after individual and dual blockades of PD-1 and CTLA-4 ( $p < 0.05$ ), except for *TIGIT* (Figure 3E). Additionally, we investigated the abundance of specific combinations of co-expressed IRs in CD8<sup>+</sup> T cells before and after ICI treatment, among which 31 possible co-expressed IR combinations were identified. Specifically, PD-1 blockade significantly boosted the co-expression levels of *PDCD1* with other IR genes, mostly represented by *PDCD1* and *LAG3*, as well as *PDCD1* and *HAVCR2*. Dual blockade of PD-1 and CTLA-4 significantly upregulated the co-expression levels of *CTLA-4* with other IR genes, mostly represented by *CTLA-4* and *LAG3*, *CTLA-4* and *PDCD1*, as well as *CTLA-4*, *LAG3*, and *PDCD1* (Figure 3F). Meanwhile, we investigated whether the co-expression pattern of multiple IRs on T cells post-immune checkpoint blockade (ICB) treatment was prevalent among all patients or limited to responders. Our findings revealed that IR co-expression pattern was present across all patients post-ICB treatment (Figure S3A). However, there was no notable difference in IR co-expression patterns between patients who responded successfully or failed to respond to ICB therapy (Figure S3B; Table S10).

Conclusively, individual and dual blockades of PD-1 and CTLA-4 significantly altered the IR expression patterns of CD8<sup>+</sup> T cells in patients with OPSCC, which was associated with enhanced anti-tumor immunity.

**ICI combination therapy promotes tumor regression without increasing hepatic and renal toxicity**

The US Food and Drug Administration has approved many immune checkpoint drugs for clinical treatment, with widely used options ranging from single anti-PD-1, anti-CTLA-4, and anti-LAG3 to combinations such as anti-PD-1 with any other ICI to improve the tumor immune response.<sup>27–29</sup> However, a significant subset of patients exhibits limited response to existing immunotherapies.<sup>30</sup> In this study, we explored the application of triple and quadruple ICI combination therapy in mice bearing OPSCC tumors to assess whether targeting more IRs would yield improved efficacy with lower toxicity. We verified the observed alterations in IR expression patterns and the associated enhancement of CD8<sup>+</sup> T cell function resulting from ICI treatment (Figure 4A). As expected, in contrast to the control group, individual ICI application (anti-PD-1, anti-CTLA-4, anti-LAG3, and anti-TIGIT), dual blockade (PD-1 + CTLA-4, LAG3 + TIGIT), triple blockade (LAG3 + TIGIT + CTLA-4), and quadruple blockade (LAG3 + TIGIT + CTLA-4 + PD-1) exacerbated enhanced effects on tumor growth (Figures 4B–4D). However, despite the lack of statistical significant, a gradually enhanced anti-tumor efficacy was observed with the co-blockade of additional ICIs (Figures 4B–4D), with tumor-bearing mice receiving a co-blockade of up to three or four IRs showing the most prominent tumor rejection.

The serum levels of alanine aminotransferase, aspartate aminotransferase, blood urea nitrogen, and creatinine were measured to assess the systemic adverse effects of the combination therapies. Notably, no significant kidney or liver injury was detected in mice receiving the combination therapies (Figure 4E). Additionally, 32 IR combinations were identified in CD8<sup>+</sup> T cells among these tumor-bearing mice receiving the combination therapies via flow cytometry (Figures 5A and S4A; Table S9). Specifically, LAG3 blockade increased the proportion of PD1<sup>+</sup> cells, whereas PD1<sup>+</sup> TIGIT<sup>+</sup> cells and CTLA4<sup>+</sup> PD1<sup>+</sup> TIGIT<sup>+</sup> TIM3<sup>+</sup> cells more or less decreased following all ICB regimens. However, the proportions of CTLA4<sup>+</sup> PD1<sup>+</sup> TIGIT<sup>+</sup> cells showed distinct responses to different ICB regimens, among which PD-1 blockade, CTLA-4 blockade, and their combination induced decreased proportions of CTLA-4<sup>+</sup> PD-1<sup>+</sup> TIGIT<sup>+</sup> cells, and vice versa.

In summary, both individual and combined blockade of ICI could promote the tumor regression without increasing hepatic and renal toxicity and alter the IR co-expression patterns in CD8<sup>+</sup> T cells in different ways.

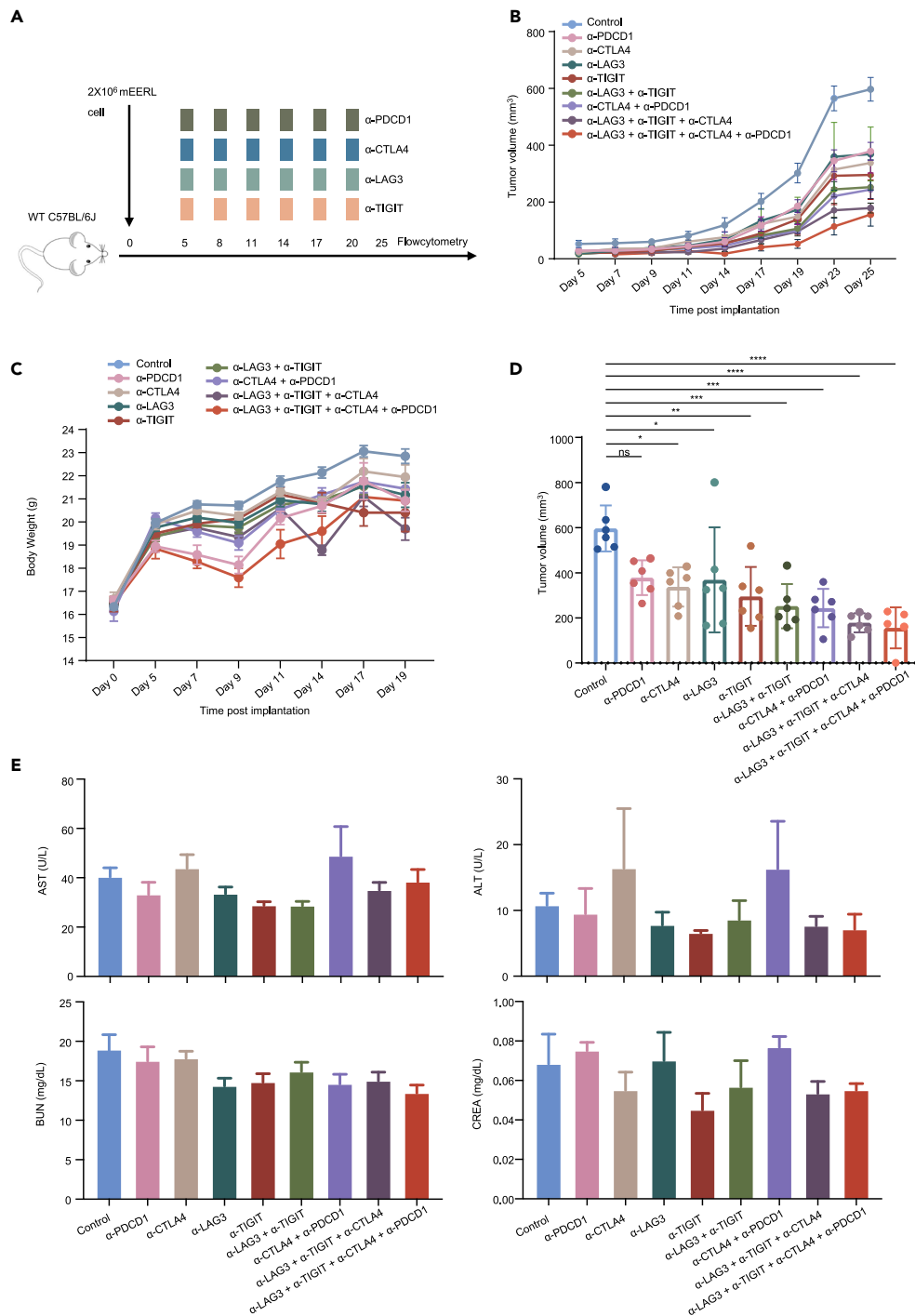


**Figure 4. ICIs combination therapy promotes tumor regression without increasing hepatic and renal toxicity**

(A) Schematic of therapeutic study design in OPSCC tumor-bearing mice. Mice were implanted with mEERL cell line and monitored for tumor growth. ICIs were administered intraperitoneally every 3 days (200 μg per treatment for α-PD-1, α-LAG3, and α-TIGIT and 100 μg per treatment for α-CTLA-4 antibody, respectively). Tumors were collected on day 25 for subsequent experiments.

(B) Tumor growth following the treatment (n = 6).

(C and D) Tumor volume following the treatment on day 25 shown by (c) representative images and (d) mean ± SEM. Statistics were assessed by Tukey's multiple comparison tests. \*p < 0.05, \*\*p < 0.01, \*\*\*p < 0.001, and \*\*\*\*p < 0.0001.

(E) Serum levels of alanine aminotransferase (ALT), aspartate aminotransferase (AST), urea nitrogen (BUN), and creatinine (CREA) following treatment (n = 6). Statistics were assessed by Tukey's multiple comparison tests.

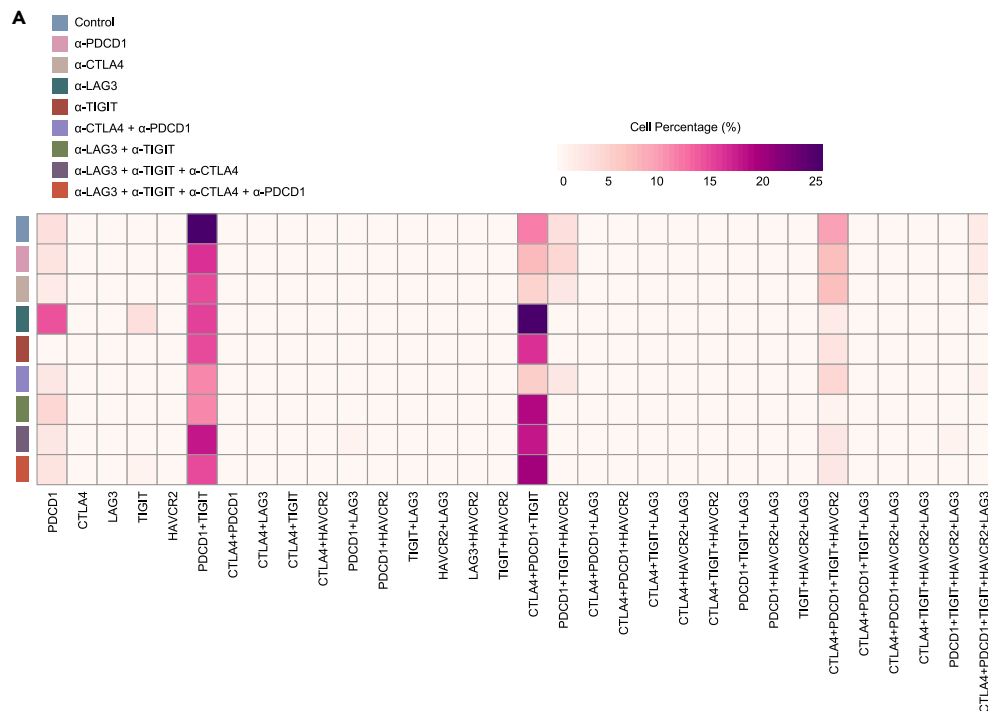


**Figure 5. The distribution patterns of co-expressed IRs in CD8<sup>+</sup> T cells following combination therapies in tumor-bearing mice**  
(A) Heatmap showing the distribution patterns of co-expressed IRs in CD8<sup>+</sup> T cells following combination therapies in tumor-bearing mice.

## DISCUSSION

Tex cells have been previously described in chronic infections and numerous types of solid tumors, largely based on their expression of various IRs.<sup>9,31</sup> However, we have a limited understanding of the functional attributes of these co-expressed IRs diversity and their implications for effective immunotherapy.

We have systematically investigated the expression patterns of various IRs in Tex cells in both human OPSCC tissues and a syngeneic OPSCC model, with the following results. First, Tex cells showed highly diverse IR co-expression patterns. Second, the number of co-expressed IRs was positively associated with superior exhaustion and cytotoxicity phenotypes. Third, in patients with OPSCC, individual and dual blockades of PD-1 and CTLA-4 redistributed the co-expression patterns of IRs; PD-1 blockade significantly boosted *PDCD1*-based co-expression with other IR genes, whereas dual blockade of PD-1 and CTLA-4 significantly upregulated *CTLA4*-based co-expression with other IR genes. These observations indicated that highly diverse IR co-expression is a leading feature of Tex cells, representing their functional state.

PD-1, a canonical IR from the CD28 superfamily, was first reported to be highly expressed and of vital importance in Tex cells.<sup>32,33</sup> Previous studies have demonstrated that the PD-1 blockade could rejuvenate Tex cells and enhance their adaptive immunity. However, functional restoration was incomplete, and defects in Tex cells remained, suggesting other negative regulatory pathways were involved.<sup>32</sup> Recent studies have identified that a PD-1<sup>+</sup>TCF1<sup>+</sup> stem-like Tex population may undergo a proliferative burst following PD-1 blockade, whereas terminal stage Tex cells co-expressing PD-1, LAG-3, and TIM3 failed to respond to this mono-ICB,<sup>15,34</sup> emphasizing the importance of dissecting the heterogeneity of IR co-expression patterns in Tex cells. Therefore, we systematically characterized the diversity of IR co-expression patterns in Tex cells in human OPSCC tissues and in a syngeneic OPSCC model. Tex cells had a high diversity of IR co-expression patterns, in which CD8<sup>+</sup> T cells co-expressing two or more IRs accounted for more than 60% of the exhausted cell population, indicating that IR co-expression is a leading feature of Tex cells in OPSCC. This partially explains why the efficacy of mono-ICBs was limited and provides a cellular basis for rational combinations of different ICIs.

A previous study based on different syngeneic tumor models showed that CD8<sup>+</sup> T cells co-expressing IRs were not dysfunctional but highly express activation and effector-related marker genes, such as *IFNG*, *GZMB*, *MKI67*, and *ICOS*. Additionally, their abundance was positively associated with tumor control and the response to PD-L1 blockade.<sup>12</sup> In a study focusing on melanoma, CD8<sup>+</sup> T cells co-expressing IRs were highly clonally expanded and proliferative,<sup>35</sup> strongly suggesting that IRs co-expression has special functional attributes for tumor-infiltrating CD8<sup>+</sup> T cells. Consistently, in this study, we confirmed that IRs were co-expressed by Tex cells in complex patterns and demonstrated that the amount of co-expressed IRs was positively associated with cytotoxic phenotypes, which is a useful predictor of effector function rather than a sign of dysfunction.

Despite the initial enthusiasm regarding the successful application of ICB in patients with cancer, the objective response rates remain modest (approximately 15%–25%) in most cohorts treated with mono-ICB.<sup>36–43</sup> Previous studies have shown the upregulation of other IRs

could be induced in tumors developing secondary resistance to ICB, which could be an immune escape mechanism.<sup>44,45</sup> Shayan et al. reported upregulation in the expression level of *HAVCR2* in T cells following anti-PD-1 therapy in head and neck cancer.<sup>44</sup> Similarly, our study demonstrated that PD-1 blockade significantly boosted the co-expression of *PDCD1* with other IR genes, mostly represented by *PDCD1* and *HAVCR2*, as well as *PDCD1* and *LAG3*. Notably, we found that the dual blockades of PD-1 and CTLA-4 significantly upregulated the co-expression levels of *CTLA-4* with other IR genes, mostly represented by *CTLA-4* and *LAG3*, *CTLA-4* and *PDCD1*, as well as *CTLA-4*, *LAG3*, and *PDCD1*, indicating a complex mechanism of immune escape following conventional ICB.

ICB, combined with additional checkpoint inhibitors, may be a prospective solution to address these challenges. Previous studies have demonstrated that the co-blockade of PD-1 and TIM3 or PD-1 and TIGIT could synergistically optimize CD8<sup>+</sup> T cell responses and partially restore the anti-tumor immunity in preclinical models.<sup>46–48</sup> Nevertheless, increasing evidence has shown interrelated relationships between the expression of various IRs, resulting in complex patterns of IR co-expression in CD8<sup>+</sup> T cells and unpredictable responses to ICB. To our knowledge, this study is the first to systematically explore the diversity of IR co-expression patterns and provide clues for the rational combinations of multiple checkpoint inhibitors.

## Conclusions

In conclusion, our findings demonstrate that highly diverse IR co-expression is a prominent feature of Tex cells and indicates their functional states, which might provide essential clues for the rational selection of ICIs in treating patients with OPSCC.

## Limitations of the study

Some limitations need to be acknowledged in this study. First, we only included 5 most canonical IRs with relatively high expression in our analysis; thus, the functional attributes of other IRs remain to be further investigated. Second, though we have observed a gradually increasing trend of anti-tumor efficacy when co-blocking more than one IR, no statistical difference was detected between those groups other than compared to the control, which need to be validated in further studies with larger sample sizes.

## STAR★METHODS

Detailed methods are provided in the online version of this paper and include the following:

- KEY RESOURCES TABLE
- RESOURCE AVAILABILITY
  - Lead contact
  - Materials availability
  - Data and code availability
- EXPERIMENTAL MODEL AND STUDY PARTICIPANT DETAILS
- METHOD DETAILS
  - OPSCC samples collection
  - Tissue dissociation and single-cell isolation
  - Single-cell gene expression and T cell receptor (TCR) repertoire sequencing
  - Single-cell RNA sequencing data processing
  - Cell type annotation
  - Definition of cytotoxicity and exhaustion and scores
  - Expression of co-inhibitory receptors on CD8<sup>+</sup> T cells
  - T cell receptors analysis
  - Trajectory inference analysis
  - Mice
  - Tumor cell line
  - Tumor implantation
  - *In vivo* treatments
  - Biochemical analysis
  - Flow cytometry
- QUANTIFICATION AND STATISTICAL ANALYSIS

## SUPPLEMENTAL INFORMATION

Supplemental information can be found online at <https://doi.org/10.1016/j.isci.2024.109668>.

## ACKNOWLEDGMENTS

We would like to thank the staff and students in the Department of Oto-Rhino-Laryngology, West China Biomedical Big Data Center, and Research Core Facility of West China Hospital for giving us kind support of sample collection and experiments. This work was supported

by the National Natural Science Foundation of China (J.R., grant #82002868, grant #82272777), West China Hospital, Sichuan University (Y. Zhao, grant #2019HXFH003; grant #ZYJC21027; Y.R., grant #2023HXBH121), the Science and Technology Department of Sichuan Province (Y. Zheng, grant #2022YFS0066), and the Sichuan Medical and Health Care Promotion Institute (X.M., grant #KY2022QN0270). The graphical abstract was created with [BioRender.com](https://BioRender.com) (agreement number: UF26K5QKAC).

## AUTHOR CONTRIBUTIONS

Y.R. and K.Q.: validation, investigation, methodology, writing – original draft, and project administration; Y.S. and M.M.: investigation, methodology, writing – original draft, and project administration; Y.W., X.C., C.J., S.W., and S.Y.: resources, investigation, and methodology; L.F., D.C., J. Li, Z.Z., Y. Zhang, J. Liu, and H.W.: investigation and methodology; X.S.: software and formal analysis; X.P.: resources and investigation; L.Y. and L.C.: resources, validation, investigation, and methodology; Y. Zheng: data curation, software, funding acquisition, and validation; W.X.: data curation, investigation, visualization, and methodology; G.L.: data curation, validation, and methodology; F.C.: resources, data curation, supervision, funding acquisition, and validation; H.Y.: resources, data curation, software, and supervision; Y. Zhao: data curation, software, supervision, funding acquisition, project administration, and writing – review and editing; J.R.: conceptualization, supervision, funding acquisition, investigation, project administration, and writing – review and editing.

## DECLARATION OF INTERESTS

The authors declare no competing interests.

Received: September 11, 2023

Revised: January 5, 2024

Accepted: April 2, 2024

Published: April 5, 2024

## REFERENCES

- Lechner, M., Liu, J., Masterson, L., and Fenton, T.R. (2022). HPV-associated oropharyngeal cancer: epidemiology, molecular biology and clinical management. *Nat. Rev. Clin. Oncol.* 19, 306–327. <https://doi.org/10.1038/s41571-022-00603-7>.
- Lechner, M., Jones, O.S., Breeze, C.E., and Gilson, R. (2019). Gender-neutral HPV vaccination in the UK, rising male oropharyngeal cancer rates, and lack of HPV awareness. *Lancet Infect. Dis.* 19, 131–132. [https://doi.org/10.1016/s1473-3099\(18\)30802-8](https://doi.org/10.1016/s1473-3099(18)30802-8).
- Faraji, F., Rettig, E.M., Tsai, H.L., El Asmar, M., Fung, N., Eisele, D.W., and Fakhry, C. (2019). The prevalence of human papillomavirus in oropharyngeal cancer is increasing regardless of sex or race, and the influence of sex and race on survival is modified by human papillomavirus tumor status. *Cancer* 125, 761–769. <https://doi.org/10.1002/cncr.31841>.
- Miyauchi, S., Kim, S.S., Pang, J., Gold, K.A., Gutkind, J.S., Califano, J.A., Mell, L.K., Cohen, E.E.W., and Sharabi, A.B. (2019). Immune Modulation of Head and Neck Squamous Cell Carcinoma and the Tumor Microenvironment by Conventional Therapeutics. *Clin. Cancer Res.* 25, 4211–4223. <https://doi.org/10.1158/1078-0432.ccr-18-0871>.
- Moy, J.D., Moskovitz, J.M., and Ferris, R.L. (2017). Biological mechanisms of immune escape and implications for immunotherapy in head and neck squamous cell carcinoma. *Eur. J. Cancer* 76, 152–166. <https://doi.org/10.1016/j.ejca.2016.12.035>.
- Ding, Q.Q., Chauvin, J.M., and Zarour, H.M. (2020). Targeting novel inhibitory receptors in cancer immunotherapy. *Semin. Immunol.* 49, 101436. <https://doi.org/10.1016/j.smim.2020.101436>.
- Anderson, A.C., Joller, N., and Kuchroo, V.K. (2016). Lag-3, Tim-3, and TIGIT: Co-inhibitory Receptors with Specialized Functions in Immune Regulation. *Immunity* 44, 989–1004. <https://doi.org/10.1016/j.immuni.2016.05.001>.
- Zarour, H.M. (2016). Reversing T-cell Dysfunction and Exhaustion in Cancer. *Clin. Cancer Res.* 22, 1856–1864. <https://doi.org/10.1158/1078-0432.ccr-15-1849>.
- Blank, C.U., Haining, W.N., Held, W., Hogan, P.G., Kallies, A., Lugli, E., Lynn, R.C., Philip, M., Rao, A., Restifo, N.P., et al. (2019). Defining 'T cell exhaustion'. *Nat. Rev. Immunol.* 19, 665–674. <https://doi.org/10.1038/s41577-019-0221-9>.
- Chow, A., Perica, K., Klebanoff, C.A., and Wolchok, J.D. (2022). Clinical implications of T cell exhaustion for cancer immunotherapy. *Nat. Rev. Clin. Oncol.* 19, 775–790. <https://doi.org/10.1038/s41571-022-00689-z>.
- Baitsch, L., Baumgaertner, P., Devèvre, E., Raghav, S.K., Legat, A., Barba, L., Wiekowski, S., Bouzourene, H., Deplancke, B., Romero, P., et al. (2011). Exhaustion of tumor-specific CD8(+) T cells in metastases from melanoma patients. *J. Clin. Invest.* 121, 2350–2360. <https://doi.org/10.1172/JCI46102>.
- Xiong, H., Mittman, S., Rodriguez, R., Pacheco-Sanchez, P., Moskalenko, M., Yang, Y., Elstrott, J., Ritter, A.T., Müller, S., Nickles, D., et al. (2019). Coexpression of Inhibitory Receptors Enriches for Activated and Functional CD8(+) T Cells in Murine Syngeneic Tumor Models. *Cancer Immunol. Res.* 7, 963–976. <https://doi.org/10.1158/2326-6066.CIR-18-0750>.
- Philip, M., Fairchild, L., Sun, L., Horste, E.L., Camara, S., Shakiba, M., Scott, A.C., Viale, A., Lauer, P., Merghoub, T., et al. (2017). Chromatin states define tumour-specific T cell dysfunction and reprogramming. *Nature* 545, 452–456. <https://doi.org/10.1038/nature22367>.
- Cheng, D., Qiu, K., Rao, Y., Mao, M., Li, L., Wang, Y., Song, Y., Chen, J., Yi, X., Shao, X., et al. (2023). Proliferative exhausted CD8(+) T cells exacerbate long-lasting anti-tumor effects in human papillomavirus-positive head and neck squamous cell carcinoma. *Elife* 12, e82705. <https://doi.org/10.7554/eLife.82705>.
- Wherry, E.J., and Kurachi, M. (2015). Molecular and cellular insights into T cell exhaustion. *Nat. Rev. Immunol.* 15, 486–499. <https://doi.org/10.1038/nri3862>.
- Zheng, C., Zheng, L., Yoo, J.K., Guo, H., Zhang, Y., Guo, X., Kang, B., Hu, R., Huang, J.Y., Zhang, Q., et al. (2017). Landscape of Infiltrating T Cells in Liver Cancer Revealed by Single-Cell Sequencing. *Cell* 169, 1342–1356.e16. <https://doi.org/10.1016/j.cell.2017.05.035>.
- St Paul, M., and Ohashi, P.S. (2020). The Roles of CD8(+) T Cell Subsets in Antitumor Immunity. *Trends Cell Biol.* 30, 695–704. <https://doi.org/10.1016/j.tcb.2020.06.003>.
- Zheng, L., Qin, S., Si, W., Wang, A., Xing, B., Gao, R., Ren, X., Wang, L., Wu, X., Zhang, J., et al. (2021). Pan-cancer single-cell landscape of tumor-infiltrating T cells. *Science* 374, abe6474. <https://doi.org/10.1126/science.abe6474>.
- Cillo, A.R., Kürten, C.H.L., Tabib, T., Qi, Z., Onkar, S., Wang, T., Liu, A., Duvvuri, U., Kim, S., Soose, R.J., et al. (2020). Immune Landscape of Viral- and Carcinogen-Driven Head and Neck Cancer. *Immunity* 52, 183–199.e9. <https://doi.org/10.1016/j.immuni.2019.11.014>.
- van der Leun, A.M., Thommen, D.S., and Schumacher, T.N. (2020). CD8(+) T cell states in human cancer: insights from single-cell analysis. *Nat. Rev. Cancer* 20, 218–232. <https://doi.org/10.1038/s41568-019-0235-4>.
- Tirosh, I., Izar, B., and Prakadan, S.M. (2016). Dissecting the multicellular ecosystem of

- metastatic melanoma by single-cell RNA-seq. *Science* 352, 189–196. <https://doi.org/10.1126/science.aad0501>.
22. Zhang, X., Peng, L., Luo, Y., Zhang, S., Pu, Y., Chen, Y., Guo, W., Yao, J., Shao, M., Fan, W., et al. (2021). Dissecting esophageal squamous-cell carcinoma ecosystem by single-cell transcriptomic analysis. *Nat. Commun.* 12, 5291. <https://doi.org/10.1038/s41467-021-25539-x>.
  23. Carlisle, J.W., Steuer, C.E., Owonikoko, T.K., and Saba, N.F. (2020). An update on the immune landscape in lung and head and neck cancers. *CA. Cancer J. Clin.* 70, 505–517. <https://doi.org/10.3322/caac.21630>.
  24. Zhou, L., Zeng, Z., Eglhoff, A.M., Zhang, F., Guo, F., Campbell, K.M., Du, P., Fu, J., Zolkind, P., Ma, X., et al. (2022). Checkpoint blockade-induced CD8+ T cell differentiation in head and neck cancer responders. *J. Immunother. Cancer* 10, e004034. <https://doi.org/10.1136/jitc-2021-004034>.
  25. Luoma, A.M., Suo, S., Wang, Y., Gunasti, L., Porter, C.B.M., Nabilsi, N., Tadros, J., Ferretti, A.P., Liao, S., Gurer, C., et al. (2022). Tissue-resident memory and circulating T cells are early responders to pre-surgical cancer immunotherapy. *Cell* 185, 2918–2935.e29. <https://doi.org/10.1016/j.cell.2022.06.018>.
  26. Berraondo, P. (2019). Mechanisms of action for different checkpoint inhibitors. *Hemisphere* 3, 28–30. <https://doi.org/10.1097/HS9.0000000000000244>.
  27. Topalian, S.L., Hodi, F.S., Brahmer, J.R., Gettinger, S.N., Smith, D.C., McDermott, D.F., Powderly, J.D., Carvajal, R.D., Sosman, J.A., Atkins, M.B., et al. (2012). Safety, activity, and immune correlates of anti-PD-1 antibody in cancer. *N. Engl. J. Med.* 366, 2443–2454. <https://doi.org/10.1056/NEJMoa1200690>.
  28. Camacho, L.H., Antonia, S., Sosman, J., Kirkwood, J.M., Gajewski, T.F., Redman, B., Pavlov, D., Bulanhagui, C., Bozon, V.A., Gomez-Navarro, J., and Ribas, A. (2009). Phase I/II trial of tremelimumab in patients with metastatic melanoma. *J. Clin. Oncol.* 27, 1075–1081. <https://doi.org/10.1200/JCO.2008.19.2435>.
  29. Ascierto, P.A., Melero, I., Bhatia, S., Bono, P., Sanborn, R.E., Lipson, E.J., Callahan, M.K., Gajewski, T., Gomez-Roca, C.A., Hodi, F.S., et al. (2017). Initial efficacy of anti-lymphocyte activation gene-3 (anti-LAG-3; BMS-986016) in combination with nivolumab (nivo) in pts with melanoma (MEL) previously treated with anti-PD-1/PD-L1 therapy. *J. Clin. Oncol.* 35, 9520. [https://doi.org/10.1200/JCO.2017.35.15\\_suppl.9520](https://doi.org/10.1200/JCO.2017.35.15_suppl.9520).
  30. Archilla-Ortega, A., Domuro, C., Martin-Liberal, J., and Muñoz, P. (2022). Blockade of novel immune checkpoints and new therapeutic combinations to boost antitumor immunity. *J. Exp. Clin. Cancer Res.* 41, 62. <https://doi.org/10.1186/s13046-022-02264-x>.
  31. Appay, V., Douek, D.C., and Price, D.A. (2008). CD8+ T cell efficacy in vaccination and disease. *Nat. Med.* 14, 623–628. <https://doi.org/10.1038/nm.f.1774>.
  32. Barber, D.L., Wherry, E.J., Masopust, D., Zhu, B., Allison, J.P., Sharpe, A.H., Freeman, G.J., and Ahmed, R. (2006). Restoring function in exhausted CD8 T cells during chronic viral infection. *Nature* 439, 682–687. <https://doi.org/10.1038/nature04444>.
  33. Sharpe, A.H., Wherry, E.J., Ahmed, R., and Freeman, G.J. (2007). The function of programmed cell death 1 and its ligands in regulating autoimmunity and infection. *Nat. Immunol.* 8, 239–245. <https://doi.org/10.1038/ni1443>.
  34. Im, S.J., Hashimoto, M., Gerner, M.Y., Lee, J., Kissick, H.T., Burger, M.C., Shan, Q., Hale, J.S., Lee, J., Nasti, T.H., et al. (2016). Defining CD8(+) T cells that provide the proliferative burst after PD-1 therapy. *Nature* 537, 417–421. <https://doi.org/10.1038/nature19330>.
  35. Li, H., van der Leun, A.M., Yofe, I., Lubling, Y., Gelbard-Solodkin, D., van Akkooi, A.C.J., van den Braber, M., Rozeman, E.A., Haanen, J.B.A.G., Blank, C.U., et al. (2019). Dysfunctional CD8 T Cells Form a Proliferative, Dynamically Regulated Compartment within Human Melanoma. *Cell* 176, 775–789.e18. <https://doi.org/10.1016/j.cell.2018.11.043>.
  36. Yap, T.A., Parkes, E.E., Peng, W., Moyers, J.T., Curran, M.A., and Tawbi, H.A. (2021). Development of Immunotherapy Combination Strategies in Cancer. *Cancer Discov.* 11, 1368–1397. <https://doi.org/10.1158/2159-8290.CD-20-1209>.
  37. Dobosz, P., and Dzieciatkowski, T. (2019). The Intriguing History of Cancer Immunotherapy. *Front. Immunol.* 10, 2965. <https://doi.org/10.3389/fimmu.2019.02965>.
  38. Twomey, J.D., and Zhang, B. (2021). Cancer Immunotherapy Update: FDA-Approved Checkpoint Inhibitors and Companion Diagnostics. *AAPS J.* 23, 39. <https://doi.org/10.1208/s12248-021-00574-0>.
  39. Ferris, R.L., Blumenschein, G., Fayette, J., Guigay, J., Colevas, A.D., Licitra, L., Harrington, K., Kasper, S., Vokes, E.E., Even, C., et al. (2016). Nivolumab for Recurrent Squamous-Cell Carcinoma of the Head and Neck. *N. Engl. J. Med.* 375, 1856–1867. <https://doi.org/10.1056/NEJMoa1602252>.
  40. Garon, E.B., Rizvi, N.A., Hui, R., Leigh, N., Balmanoukian, A.S., Eder, J.P., Patnaik, A., Aggarwal, C., Gubens, M., Horn, L., et al. (2015). Pembrolizumab for the Treatment of Non-Small-Cell Lung Cancer. *N. Engl. J. Med.* 372, 2018–2028. <https://doi.org/10.1056/NEJMoa1501824>.
  41. Motzer, R.J., Escudier, B., McDermott, D.F., George, S., Hammers, H.J., Srinivas, S., Tykodi, S.S., Sosman, J.A., Procopio, G., Plimack, E.R., et al. (2015). Nivolumab versus Everolimus in Advanced Renal-Cell Carcinoma. *N. Engl. J. Med.* 373, 1803–1813. <https://doi.org/10.1056/NEJMoa1510665>.
  42. Rosenberg, J.E., Hoffman-Censits, J., Powles, T., van der Heijden, M.S., Balar, A.V., Necchi, A., Dawson, N., O'Donnell, P.H., Balmanoukian, A., Loriot, Y., et al. (2016). Atezolizumab in patients with locally advanced and metastatic urothelial carcinoma who have progressed following treatment with platinum-based chemotherapy: a single-arm, multicentre, phase 2 trial. *Lancet (N. Am. Ed.)* 387, 1909–1920. [https://doi.org/10.1016/S0140-6736\(16\)00561-4](https://doi.org/10.1016/S0140-6736(16)00561-4).
  43. El-Khoueiry, A.B., Sangro, B., Yau, T., Crocenzi, T.S., Kudo, M., Hsu, C., Kim, T.Y., Choo, S.P., Trojan, J., Welling, T.H., et al. (2017). Nivolumab in patients with advanced hepatocellular carcinoma (CheckMate 040): an open-label, non-comparative, phase 1/2 dose escalation and expansion trial. *Lancet (N. Am. Ed.)* 389, 2492–2502. [https://doi.org/10.1016/S0140-6736\(17\)31046-2](https://doi.org/10.1016/S0140-6736(17)31046-2).
  44. Shayan, G., Srivastava, R., Li, J., Schmitt, N., Kane, L.P., and Ferris, R.L. (2017). Adaptive resistance to anti-PD1 therapy by Tim-3 upregulation is mediated by the PI3K-Akt pathway in head and neck cancer. *Oncol Immunology* 6, e1261779. <https://doi.org/10.1080/2162402X.2016.1261779>.
  45. Anderson, A.C., Anderson, D.E., Bregoli, L., Hastings, W.D., Kassam, N., Lei, C., Chandwaskar, R., Karman, J., Su, E.W., Hirashima, M., et al. (2007). Promotion of tissue inflammation by the immune receptor Tim-3 expressed on innate immune cells. *Science* 318, 1141–1143. <https://doi.org/10.1126/science.1148536>.
  46. Sakuishi, K., Apetoh, L., Sullivan, J.M., Blazar, B.R., Kuchroo, V.K., and Anderson, A.C. (2010). Targeting Tim-3 and PD-1 pathways to reverse T cell exhaustion and restore antitumor immunity. *J. Exp. Med.* 207, 2187–2194. <https://doi.org/10.1084/jem.20100643>.
  47. Kim, J.E., Patel, M.A., Mangraviti, A., Kim, E.S., Theodoros, D., Velarde, E., Liu, A., Sankey, E.W., Tam, A., Xu, H., et al. (2017). Combination Therapy with Anti-PD-1, Anti-TIM-3, and Focal Radiation Results in Regression of Murine Gliomas. *Clin. Cancer Res.* 23, 124–136. <https://doi.org/10.1158/1078-0432.CCR-15-1535>.
  48. Banta, K.L., Xu, X., Chitre, A.S., Au-Yeung, A., Takahashi, C., O'Gorman, W.E., Wu, T.D., Mittman, S., Cubas, R., Comps-Agrar, L., et al. (2022). Mechanistic convergence of the TIGIT and PD-1 inhibitory pathways necessitates co-blockade to optimize anti-tumor CD8(+) T cell responses. *Immunity* 55, 512–526.e9. <https://doi.org/10.1016/j.immuni.2022.02.005>.
  49. Guo, X., Zhang, Y., Zheng, L., Zheng, C., Song, J., Zhang, Q., Kang, B., Liu, Z., Jin, L., Xing, R., et al. (2018). Global characterization of T cells in non-small-cell lung cancer by single-cell sequencing. *Nat. Med.* 24, 978–985. <https://doi.org/10.1038/s41591-018-0045-3>.

**STAR★METHODS**

**KEY RESOURCES TABLE**

REAGENT or RESOURCE	SOURCE	IDENTIFIER
<b>Chemicals, peptides, and recombinant proteins</b>		
DMEM Medium	Gibco	Cat#: C11995500BT
Penicillin-Streptomycin solution	Hyclone	Cat#: SV30010
HBSS	Gibco	Cat#: 14025092
Bovine Serum Albumin	Sigma-Aldrich	Cat#: 05470
CD3 MicroBeads, human	Miltenyi Biotec	Cat#: 130-050-101
Tumor Dissociation Kit, human	Miltenyi Biotec	Cat#: 130-095-929
Tumor Dissociation Kit, mouse	Miltenyi Biotec	Cat#: 130-096-730
MS Separation columns	Miltenyi Biotec	Cat#: 130-042-201
Zombie NIR Fixable Viability Kit	Biolegend	Cat#: 423106; RRID: AB_3096190
Alexa Fluor® 700 anti-mouse CD3	Biolegend	Cat#: 100216; RRID: AB_493696
Pacific Blue™ anti-mouse CD8a	Biolegend	Cat#: 100725; RRID: AB_493425
Brilliant Violet 605™ anti-mouse CD366 (Tim-3)	Biolegend	Cat#: 119721; RRID: AB_2616907
FITC anti-mouse CD279 (PD-1)	Biolegend	Cat#: 135213; RRID: AB_10689633
Brilliant Violet 650™ anti-mouse CD223 (LAG-3)	Biolegend	Cat#: 125227; RRID: AB_2687209
PE/Dazzle™ 594 anti-mouse TIGIT (Vstm3)	Biolegend	Cat#: 142110; RRID: AB_2566572
APC anti-mouse CD152(CTLA4)	Biolegend	Cat#: 106310; RRID: AB_2087653
PE/Cyanine5 anti-human/mouse GZMB Recombinant	Biolegend	Cat#: 372226; RRID: AB_3096191
BUV395 Rat Anti-Mouse CD45(30-F11)	BD Biosciences	Cat#: 565967; RRID: AB_2651134
Chromium Single Cell 5' Library Construction Kit	10x Genomics	Cat#: PN-1000020
Chromium Single Cell 5' Library & Gel Bead Kit	10x Genomics	Cat#: PN-1000006
Chromium Single Cell V(D)J Enrichment Kit	10x Genomics	Cat#: PN-1000005
Prigrow IV Medium	abm	Cat#: TM004
InVivoMAb anti-mouse PD-1	BioXcell	Cat#: BE0273; RRID: AB_2687796
InVivoMAb anti-mouse CTLA-4	BioXcell	Cat#: BE0131; RRID: AB_10950184
InVivoMAb anti-mouse LAG-3	BioXcell	Cat#: BE0174; RRID: AB_10949602
InVivoMAb anti-mouse TIGIT	BioXcell	Cat#: BE0274; RRID: AB_2687797
<b>Deposited data</b>		
The raw scRNA-seq and scTCR-seq data	This paper	<a href="http://bigd.big.ac.cn/gsa-human">http://bigd.big.ac.cn/gsa-human</a> : HRA003921
scRNA-seq of patients with OPSCC	GEO	GEO: GSE200996
<b>Experimental models: Cell lines</b>		
mEERL cell line	abm	T8309; RRID: CVCL_B6J3
<b>Experimental models: Organisms/strains</b>		
C57Bl/6J	Byrness Weil Biotech Ltd	N/A
<b>Software and algorithms</b>		
Cell Ranger count	10x Genomics	v3.0.2
Cell Ranger VDJ	10x Genomics	v6.1.1
Seurat	R	v4.1.2
monocle3	R	v1.2.4
scRepertoire	R	v1.3.5
FlowJo	BD Biosciences	v10.8.1
GraphPad Prism		v8.4.2

## RESOURCE AVAILABILITY

### Lead contact

Further information and requests for resources and reagents should be directed to and will be fulfilled by the lead contact, Jianjun Ren ([Jianjun.Ren@scu.edu.cn](mailto:Jianjun.Ren@scu.edu.cn)).

### Materials availability

This study did not generate any unique new reagent. All reagents used in this study are commercially available.

### Data and code availability

- The raw sequence data are available on the Genome Sequence Archive for Human (GSA), a component of the National Genomics Data Center, with the accession number HRA003921 (<http://bigd.big.ac.cn/gsa-human>). This study analyzed publicly available data from the Gene Expression Omnibus (GEO: GSE200996) and the code is accessible from the corresponding author upon request.
- These paper does not report original code.
- All authors have approved the experiments and all experiments conform to the relevant regulatory standards.
- Any additional information required to reanalyze the data reported in this paper is available from the [lead contact](#) upon request.

## EXPERIMENTAL MODEL AND STUDY PARTICIPANT DETAILS

All animal experiments were approved by the Animal Ethics Committee of the West China Hospital (approval number:20220511001). The experiments complied with the ethical guidelines of the Guide for the Care and Use of Laboratory Animals set by the China Association of Laboratory/Animal Care, and the animals were humanely euthanized at defined endpoints.

This study was conducted in accordance with the Declaration of Helsinki (as revised in 2013) and was approved by the Biomedical Research Ethics Committee of West China Hospital (2021-908), with the individual consent for each participant.

## METHOD DETAILS

### OPSCC samples collection

This study was approved by the Ethics Committee of the West China Hospital of Sichuan University (approval number: 2021-908). All patients provided informed consent and did not undergo chemotherapy or radiotherapy before surgery. The tissue samples collected were analyzed for HPV status using droplet digital PCR (Bio-Rad, USA). The samples were obtained from nine patients with OPSCC, comprising eight primary tumor tissues and five adjacent normal tissues ([supplemental information, Table S1](#)).

### Tissue dissociation and single-cell isolation

Fresh OPSCC tumors and matched adjacent normal tissue samples were placed on ice following surgical resection in Dulbecco's modified eagle medium (DMEM, USA), supplemented with 1% Penicillin/Streptomycin solution (Hyclone, USA). Subsequently, all samples were gently cut into small pieces on ice and digested using a tumor dissociation kit (Miltenyi Biotec, Germany), following the built-in program 37C\_h\_TDK\_3 for tumor tissues and program 37C\_h\_TDK\_1 for adjacent normal tissues. After disruption, the cells were filtered through a 40 mm filter (BD Biosciences, USA) and washed with 1x Hank's balanced salt solution (HBSS, USA). The resulting single-cell suspension was centrifuged at 500G for 5 minutes and resuspended in 4% bovine serum albumin (BSA, USA). Single-cell suspensions were then stained with CD3 MicroBeads (Miltenyi Biotec, Germany) and sorted into immune (CD3<sup>+</sup>) cells via magnetic separation using MS Separation columns (Miltenyi Biotec, Germany). Cell number and viability were checked after staining with 0.4% trypan blue staining (cell number > 5 × 10<sup>5</sup> and viability > 80%).

### Single-cell gene expression and T cell receptor (TCR) repertoire sequencing

The sorted immune cells were encapsulated and loaded onto each channel of the Chromium Controller (10x Genomics). After droplet encapsulation, single-cell cDNA synthesis, amplification, and sequencing, libraries were constructed using Chromium Single Cell 5' Library Construction Kit (10x Genomics), Chromium Single Cell 5' Library & Gel Bead Kit (10x Genomics), and Chromium Single Cell V(D)J Enrichment Kit, Human T Cell (10x Genomics). The completed libraries were sequenced on the Illumina NovaSeq 6000 platform.

### Single-cell RNA sequencing data processing

Raw scRNA-sequencing reads were demultiplexed into FASTQ files using Cell Ranger Count (10x Genomics, v3.0.2) and aligned to the GRCh38 reference genome using default parameters. Raw gene expression matrices were generated for each sample and input into the R package Seurat (v4.1.2) for downstream analysis.

Low-quality cells were removed by eliminating genes whose expression was detected in < 0.1% of all cells and in cells with gene counts < 200 or mitochondrial RNA content > 10%. Genes displaying highly variable expressions were selected based on the average

expression and dispersion level thresholds using the *FindVariableGenes* function with default settings. Normalization of the expression level for each gene involved linear regression against the total UMI counts and mitochondrial RNA content per cell using the *ScaleData* function, and principal component analysis (PCA) was conducted using the *RunPCA* function. The DoubletFinder package (v2.0.3) was used to detect and remove estimated doublet cells, and batch corrections were performed across different patients using the *RunHarmony* function of the Harmony package (v0.1.0). Then top 30 principal components were selected to performed graph-based Louvain clustering using the *FindClusters* function (resolution = 1.0).

### Cell type annotation

The 23,867 extracted CD8<sup>+</sup> T cells were used for further clustering analysis, and 10 sub-clusters were generated (*FindClusters*, resolution = 0.6). With default parameters, the *FindAllMarkers* function of Seurat was used to identify differentially expressed genes (DEGs) in different sub-clusters (Table S2). All sub-clusters were identified using the top-ranked DEGs of each cluster and canonical cell type-specific gene markers. To visualize the single cell transcriptional profile in 2D space, uniform manifold approximation and projection (UMAP) was finally applied based on the described shared nearest neighbor (SNN) graph.

### Definition of cytotoxicity and exhaustion and scores

The cytotoxicity signature was derived from DEGs across all CD8<sup>+</sup> T cell subtypes. The reference gene, *PRF1*, along with other genes in CD8<sup>+</sup> T cells, were analyzed using Pearson's correlation with scaled expression values. The genes (*PRF1*, *GZMB*, *GZMH*, *GNLY*, *GZMA*, *CCL5*, *KLRD1*, *LGALS3*, *KLRC1*, *IL2RG*, *HLA-DRB1*, *CXCR6*, *IFITM2*, *CD63*, *CST7*) with the highest correlation to the reference gene were defined as signature cytotoxic genes. Subsequently, using the *AddModuleScore* function, the cytotoxicity signature scores for individual cells were computed.<sup>21,22,49</sup> For the exhaustion score, the *PDCD1* gene was chosen as the reference gene to define the exhaustion signature (*PDCD1*, *CXCL13*, *CTLA-4*, *HAVCR2*, *ENTPD1*, *LAG3*, *RGS1*, *TIGIT*, *ITGAE*, *LAYN*, *TOX*) using the same method.

### Expression of co-inhibitory receptors on CD8<sup>+</sup> T cells

Based on the expression levels of these IR signatures (*PDCD1*, *CTLA-4*, *HAVCR2*, *LAG3*, and *TIGIT*) in CD8<sup>+</sup> T cells, 32 mutually exclusive combinatorial expression patterns were identified in a mutually exclusive manner. IR-0 denotes a cell cluster with no detected IRs, IR-1 denotes a cell cluster with only one expressed IR, and so on. IR-2–IR-5 represent different cell clusters wherein any two to five IRs combination were expressed.

### T cell receptors analysis

The TCR sequences of individual cells were processed using the Cell Ranger V(D)J (10x Genomics, v6.1.1) and aligned to the reference cell-ranger-vdj-GRCh38-alt-ensembl-5.0.0, with the default parameters. Each unique TCR sequence was defined as a clonotype, and T cells derived from the same cell clone were considered to share the same clonotype. Clonotype frequency matrices of each sample were integrated with scRNA-seq data for further analysis via the scRepertoire R package (v1.3.5). The total frequency assigned for different extents of clonal expansion was categorized as follows: Hyperexpanded ( $20 < X \leq 200$ ), Multiple ( $2 < X \leq 20$ ), Double ( $1 < X \leq 2$ ), Single ( $0 < X \leq 1$ ).

### Trajectory inference analysis

We defined the imputed pseudotime trajectories in CD8<sup>+</sup> T cells using the monocle3 R package (v1.2.4). The UMAP matrix obtained from the clustering analysis was input into *cluster\_cells* and *learn\_graph* functions, and the IL7R<sup>+</sup> CD8<sup>+</sup> T cell cluster (cluster C2) was set as the root state for evaluating the cell trajectories.

### Mice

Male C57Bl/6J mice (6–8 weeks) were purchased from Byrness Weil Biotech Ltd (Chongqing, China) and kept in a pathogen-free environment with ambient temperature of  $20 \pm 4^\circ\text{C}$ , a relative humidity of  $60 \pm 5\%$ , and a 12-hour light/dark cycle. All animal experiments were approved by the Animal Ethics Committee of the West China Hospital (approval number: 20220511001). The experiments complied with the ethical guidelines set by the Guide for the Care and Use of Laboratory Animals of the China Association of Laboratory/Animal Care, and the animals were humanely euthanized at defined endpoints.

### Tumor cell line

The mEERL cell line, derived from mouse tonsil epithelial cells expressing the HPV-16 E6, E7 and *Ras* genes, was purchased from Applied Biologic Materials (abm, Richmond, Canada). The mEERL cells were cultured in Prigrow IV medium (abm), comprising 10% fetal bovine serum, 0.5  $\mu\text{g}/\text{mL}$  hydrocortisone, 5  $\mu\text{g}/\text{mL}$  transferrin, 5  $\mu\text{g}/\text{mL}$  insulin, 1.36 ng/mL tri-iodo-thyronine, 5 ng/mL epidermal growth factor, and 1% Penicillin/Streptomycin Solution. Stocks of mEERL were generated upon cell reception and used for tumor experiments. All cells were tested regularly for mycoplasma contamination, and showed consistent negative results.

### Tumor implantation

Mice were subcutaneously injected with  $2 \times 10^6$  mEERL cells subcutaneously in 100  $\mu$ L PBS on the right flank. Tumors were measured every 2–3 days using digital calipers, and tumor volume was estimated using the formula: (tumor volume =  $\pi/6 \times \text{length} \times \text{width}^2$ ). The animals were euthanized when the tumor volumes exceeded 1,000  $\text{mm}^3$ .

### In vivo treatments

Tumor-bearing mice were treated intraperitoneally with anti-PD1 (Rat IgG2a, clone 29F.1A12, BioXcell, 200  $\mu$ g per dose), anti-CTLA-4 (Syrian Hamster IgG, clone 9H10, BioXcell, 100  $\mu$ g per dose), anti-LAG3 (Rat IgG1, clone C9B7W, BioXcell, 200  $\mu$ g per dose), or anti-TIGIT (Mouse IgG1, k, clone 1G9, BioXcell, 200  $\mu$ g per dose) every 3 days, starting on the day 5.

### Biochemical analysis

Blood samples were collected from the retro-orbital plexus of tumor-bearing mice on day 25. ALT, AST, BUN, and CREA levels in the serum were immediately measured using a Roche Cobas c702 analyzer. The data collected were analyzed using the GraphPad Software (v8.4.2).

### Flow cytometry

The tumors were collected and cut into small pieces (2–4 mm). Following the manufacturer's recommendation, the samples were then dissociated into single cell suspensions using a Tumor Dissociation Kit (Miltenyi Biotec, Germany). For CD8<sup>+</sup> T cell analysis, cell viability was assessed with LIVE/DEAD Fixable Viability Stain kit (BioLegend, USA) for 30 minutes at 4°C. Cells were then simultaneously stained with the following surface antibodies: AF700-CD3 (clone 17A2), Pacific Blue-CD8a (clone 53-6.7), BV605-HAVCR2 (clone RMT3-23), FITC-PD1 (clone 29F.1A12), BV650-LAG3 (clone C9B7W), PE/Dztle 594-TIGIT (clone 1G9), APC-CTLA4 (clone UC10-4B9) purchased from BioLegend, and BUV395-CD45 (clone 30-F11) purchased from BD Biosciences (USA). Following a 30-minute incubation at 4°C, cells were washed twice in cell staining buffer, fixed, and permeabilized using the Transcription Factor Buffer Set (BD Biosciences). The fixed cells were washed and intracellularly stained with an optimum concentration of PE/Cyanine5-GZMB (clone QA16A02, Biolegend) for 50 minutes in the dark at 4°C. After washing twice, the cells were resuspended in PBS and measured using a BD FACSAria SORP Flow Cytometer. Data collected were analyzed using FlowJo v10.8.1 (BD Biosciences).

### QUANTIFICATION AND STATISTICAL ANALYSIS

Statistical analyses were performed using GraphPad Prism (<https://www.graphpad.com/>) for experimental data, and R (v4.1.2) for sequencing data. Unless otherwise mentioned, Tukey's multiple comparison test was used for statistical analysis. Significance was achieved when  $p < 0.05$  or the adjusted  $p$ -value  $< 0.05$ , where appropriate.